

# Comparison of wave-body interaction modelling methods for the study of reactively controlled point absorber wave energy converter

Boyin Ding<sup>1</sup>, Pierre-Yves Wuillaume<sup>2</sup>, Fantai Meng<sup>1</sup>, Aurélien Babarit<sup>2</sup>, Benjamin Schubert<sup>1</sup>,  
Nataliia Sergiienko<sup>1</sup>, Benjamin Cazzolato<sup>1</sup>

<sup>1</sup>Ocean Wave Energy Research Group, Faculty of Engineering, Computer and Mathematical Sciences, the University of Adelaide, Australia, [boyin.ding@adelaide.edu.au](mailto:boyin.ding@adelaide.edu.au)

<sup>2</sup>Ocean Waves and Marine Renewable Energy Group, LHEEA, Ecole Centrale de Nantes - CNRS, France, [aurelien.babarit@ec-nantes.fr](mailto:aurelien.babarit@ec-nantes.fr)

## 1. INTRODUCTION

Ocean waves are a huge resource of renewable energy for utilisation. Wave energy converter (WEC) devices are being developed to enable capture of this energy resource. In the late 1980s, the principle of extraction energy from waves was studied (Falnes, 2007) and it showed that reactive control can increase significantly wave power extraction for a heaving point-absorber. Since then, studies on the control strategies and their implementations have been a focus in the field of wave energy research (Ringwood, 2014).

Majority of the wave energy control studies used linear potential flow theory and Cummins equation as the basis for modelling hydrodynamics arising from wave-body interaction, which is essential for the implementation of control simulation as well as for the formulation of model-based control strategies (Penalba, 2016). Although this simplifies/linearises the control problem as well as speeds up the simulation process, the utilisation of linear solver (which assumes that the wave steepness and body motion are both small) contradicts the large motion arising from the reactively controlled wave energy converter and thus does not ensure the fidelity of the control simulation results in medium to large wave conditions. On the extreme opposite, the Navier-Stokes equation based CFD captures the full nonlinear hydrodynamics in the wave-body interaction problem leading to high fidelity simulation results regardless of the system operational conditions, however, is barely used in the study of wave energy converter control due to its high computational requirement. Compromise between the linear method and the Navier-Stokes solver also exists (Wuillaume, 2019). A typical example is the weak-scatterer potential flow method proposed for seakeeping analysis of ship with forward speed (Pawlowski, 1991), which is formulated based on the assumption that the perturbation wave field generated by the body oscillation is small compared to the incident wave field, such as the free surface conditions can be linearised at the incident wave elevation level. The weak-scatterer method takes into account the unsteady and nonlinear hydrodynamic loads associated with dynamic wave-body interaction as long as the aforementioned assumption is satisfied and that viscosity effects remain negligible. However, it remains questionable if the weak-scatterer method is suitable for solving wave energy converter control problem where large perturbation wave field is expected given the large resonant motion of the body. A further simplified version of the weak-scatterer method is the body-exact potential method that assumes the free surface conditions can be linearised around the mean free surface elevation  $z = 0$ . This solver was proposed to account for the body motion induced nonlinearities but is only valid when small steepness waves are present. It is a compromise between the weak-scatterer method and the linear method.

The proposed study intends to conduct a comparison study on the aforementioned four wave-body interaction modelling methods in terms of their fidelity in solving the reactive control problem of a submerged point-absorber (PA) WEC.

## 2. WAVE-BODY INTERACTION MODELLING METHODS

Table 1 summarises the main differences between the four wave-body interaction modelling methods.

**1) Navier-Stokes equation (CFD) solver:** Navier-Stokes equations are a set of partial differential equations that describe the motion of fluids as a relationship between flow velocity (or momentum) and pressure. For the incompressible sea water, the Navier-Stokes equations can be written in the general form as:

$$\rho \left( \frac{\partial \mathbf{u}}{\partial t} + \mathbf{u} \cdot \nabla \mathbf{u} \right) = -\nabla p + \nabla \cdot (\mu \nabla \mathbf{u}) + \mathbf{f} \quad (1a)$$

$$\nabla \cdot \mathbf{u} = 0 \quad (1b)$$

where  $\mathbf{u}$ ,  $\rho$ ,  $p$ ,  $\mu$  and  $\mathbf{f}$  are the velocity vector, density, pressure, dynamic viscosity and external force (e.g. gravity force) and  $\nabla$  is the gradient operator. Solving Equation (1) stepwise across the computational domain of the numerical wave tank under boundary conditions and integrating the total stress over the wetted body surface  $S_B(t)$  result in the total hydrodynamic force acting on the body (Meng, 2017). The advantage of CFD solvers are that they are not based on any linearisation assumption, take into account the real fluid viscosity, can accommodate turbulence effects and other nonlinear phenomena that may occur during a simulation. However, these benefits come at a cost of high level of complexity and very high computation time relative to linear models. In this study, the OpenFOAM package (e.g. OLAFOAM and interFoam utility) forms the CFD solver (specifically the Reynold-averaged Navier-Stokes model) as described by Meng et al. (2017).

**2) Weak-scatterer potential flow (WSP) solver:** The potential flow theory was established based on the assumptions that the fluid is irrotational, incompressible and inviscid. Without considering the viscosity and turbulence, the potential flow theory introduced the velocity potential  $\phi$ , the only one scalar function that is necessary to compute the three dimensional fluid velocity. Thus, the velocity potential can be evaluated using a boundary element method and the total pressure can be solved from the Bernoulli's equation (Wuillaume, 2019):

$$p = -\rho \left( \frac{\partial \phi}{\partial t} + \frac{1}{2} \nabla \phi \cdot \nabla \phi + gz \right) \quad (2)$$

where  $-\rho gz$  is the hydrostatic pressure. The total dynamic force acting on the body is then calculated by integrating the total pressure over the instantaneous wetted surface of the body  $S_B(t)$ . Due to the high computational demand associated with the fully nonlinear potential flow method in solving the real varying intersection curves between the free surface and bodies, decomposition of the velocity potential and the wave elevation into incident and perturbed quantities were applied and the weak-scatterer hypothesis was proposed (Pawlowski et al., 1991). It assumed the perturbed quantities are small compared to the incident quantities:

$$\begin{cases} \phi = \phi^I + \phi^P \\ \phi^P = \mathcal{O}(\phi^I) \end{cases} \quad (3)$$

In this case, the free surface boundary equations are linearised around the known incident free surface elevation  $z = \eta^I(x, y, t)$ . Thus, the perturbed waves are not required to be meshed which largely reduce computational demand. Due to the free surface conditions, wave breaking cannot be modelled. In this study, the *WS\_CN* numerical tool as described in detail by Wuillaume (2019) will be used as the WSP solver.

**3) Body-exact potential flow (BEP) solver:** The potential flow theory based solver can be further simplified under small wave conditions (e.g. wave steepness,  $\epsilon \ll 1$ ). Thus, the free surface conditions can be linearised around the mean surface elevation  $z = 0$ . This forces the free surface mesh remain planar, which enables a faster mesh convergence and reduction of computing time. The pressure is integrated over the wetted body surface  $S_B(t)$  subject to "body-exact" motion and delimited by the mean wave elevation. In the *WS\_CN* numerical tool, an option of linearising the free surface conditions around the mean surface elevation exists and thus the *WS\_CN* numerical tool can be configured as the BEP solver for use in this study.

**4) Linear potential flow (LP) solver:** The potential flow theory based solver can be simplified to its neatest form, by assuming that wave steepness,  $\epsilon$ , is small and the body undergoes small amplitude motion,  $A_m$ . Consequently, the free surface conditions can be linearised around the mean free surface elevation  $z = 0$  and the body meshes are fixed at the rest position of the body. This leads to a linearised model, where the perturbed component can be further decomposed into a diffraction component and a radiation component:

$$\begin{cases} \phi = \phi^I + \phi^D + \phi^R \\ \epsilon \ll 1, A_m \ll 1 \end{cases} \quad (4)$$

The elementary problems for these velocity potentials are solved and the total hydrodynamic force is obtained by summing the excitation force and the radiation force. The linearised model can be solved either in the time domain (Cummins, 1962) or in the frequency domain, with hydrodynamic functions/coefficients (e.g. added mass, radiation damping and excitation force) pre-calculated using boundary element solver (e.g. WAMIT, NEMOH, Aquaplus). Surface piercing (e.g. when a fully submerged buoy pierces the free surface) cannot be modelled in this case given the linearised surface and body conditions. In this study, a frequency-domain based linear solver is applied (Ding, 2018).

**Table 1. Main differences between the four wave-body interaction modelling methods**

	<b>Linear potential flow solver</b>	<b>Body-exact potential flow solver</b>	<b>Weak-scatterer potential solver</b>	<b>Navier-Stokes based CFD solver</b>
Assumption	$\left\{ \begin{array}{l} \text{Irrotational and} \\ \text{inviscid fluid,} \\ \epsilon \ll 1, \\ A_m \ll 1 \end{array} \right.$	$\left\{ \begin{array}{l} \text{Irrotational and} \\ \text{inviscid fluid,} \\ \epsilon \ll 1 \end{array} \right.$	$\left\{ \begin{array}{l} \text{Irrotational and} \\ \text{inviscid fluid,} \\ \phi^P = \mathcal{O}(\phi^I) \end{array} \right.$	Isotropic fluid
Hydrodynamics decomposition	$\phi = \phi^I + \phi^D + \phi^R$	$\phi = \phi^I + \phi^P$		NA
Meshed free surface	$z = 0$		$z = \eta^I(x, y, t)$	$z = \eta(x, y, t)$
Meshed body surface	$S_B(0)$	$S_B(t)$		
Hydrodynamic force computation	Sum of excitation and radiation forces	Integration of total pressure over the wetted body surface		Integration of total stress over the wetted body surface
Fluid vortices	NO			YES
Wave breaking	NO			YES
Drag force	NO, a Morison-like term $-0.5\rho C_D A  \dot{z}_b - \dot{z}_f  (\dot{z}_b - \dot{z}_f)$ can be added		YES	
Surface piercing	NO	YES		
Computational speed	Extremely fast	Medium	Slow	Extremely slow

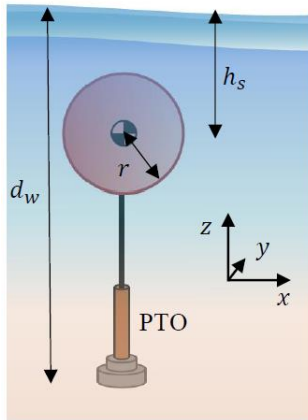


**Fig. 1. Submerged heaving PA WEC**

**Table 2. Parameters for the case studies**

Symbol	Value/unit	Description
$d_w$	50m	Water depth
$h_s$	8.5m	Submergence depth from buoy geometric centre to water surface
$r$	5m	Radius of the spherical buoy
$m$	$2.68 \times 10^5 \text{kg}$	Buoy mass, defined as half of the buoy buoyancy force $m = \rho V / 2$

### 3 CASE STUDIES

Fig. 1 shows the test case, a fully submerged heaving PA WEC with parameters defined in Table 2. A submerged PA was selected since Sergiienko et al. (2018) showed that reactive control plays a critical role in enlarging the absorption bandwidth of this PA system. A spherical buoy was selected to avoid nonlinearities associated with fluid vortices neglected by the potential flow solvers. The power take-off (PTO) was simplified as a combination of a spring, a damper, and a pretension force that counteracts the net buoyancy force. The PA system modelled by the four wave-body interaction methods was tested under regular wave conditions of 0.1m and 1m wave amplitudes and 4 typical wave frequencies, respectively. The PTO spring and damper parameters were optimised in the linear frequency-domain solver so that the PTO damper absorbed power was maximised subject to a body motion constraint of 3m (Ding, 2018). This mitigated the occurrence of surface piercing which was not accounted for by the linear solver. The optimised PTO parameters were then used by all four wave-body interaction models for a comparison. Quadratic damping was considered as an external force in the three potential flow theory based solvers to account for the drag force neglected by the inviscid fluid assumption. Fluid velocity was assumed to be zero in the Morison force computation due to its negligible influence. Lorentz linearisation was used to convert the quadratic Morison equation into a linearised damping for use in the frequency-domain linear solver (Ding, 2018).

### 4. RESULTS

Fig. 2 shows the RAO and power absorption of the heaving buoy at two wave steepness and four typical wave frequencies, output by the four wave-body interaction models. At low wave steepness (e.g. 0.1m

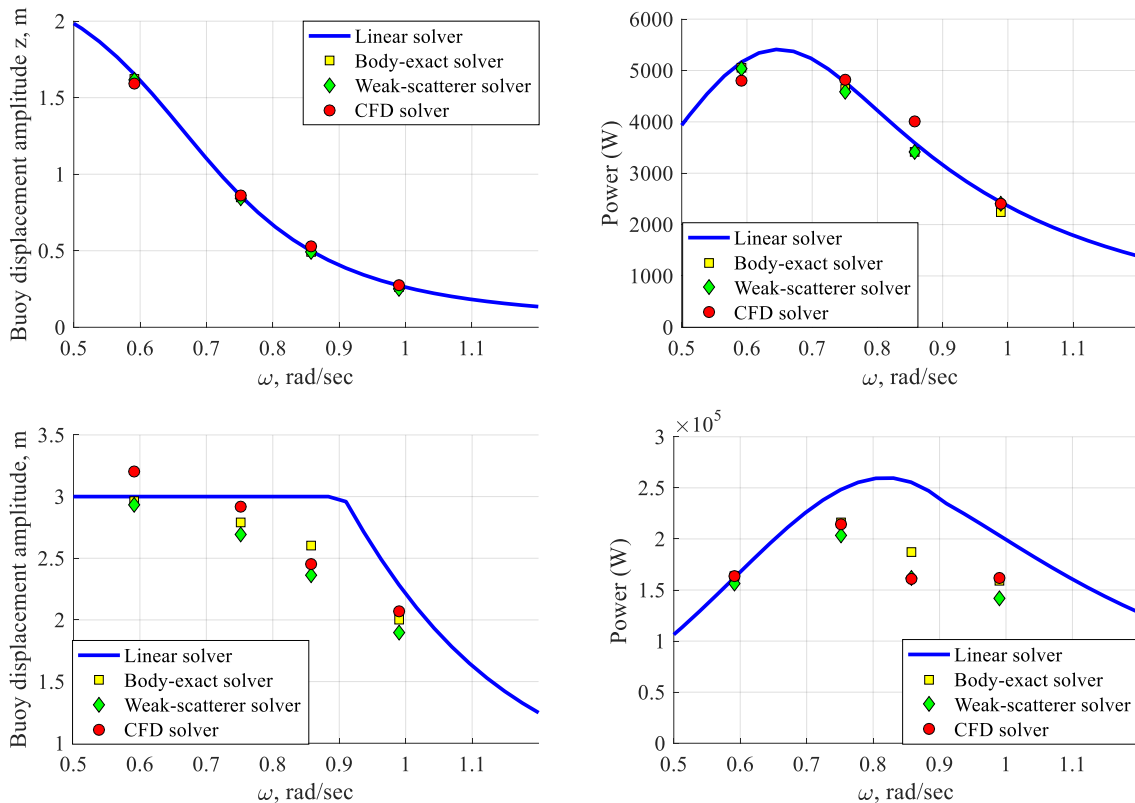


**Fig. 2. Buoy heave RAO (left) and power absorption (right) under 0.1m (upper) and 1m (lower) amplitude wave**

amplitude), the buoy RAO did not reach the 3m displacement constraint so that the buoy was kept fully submerged during its free motion. In this scenario, the buoy RAO results output by the four solvers reached a good agreement across the frequencies whilst a discrepancy of 14% in the power absorption can be observed between the CFD solver result and the potential flow solver results at 0.85rad/s. The reason behind this discrepancy is under investigation. At high wave steepness (e.g. 1m amplitude), the buoy RAOs were near the 3m displacement constraint, meaning that the buoy moved very closely to the trough of the free surface at its upper stroke so that surface piercing and wave breaking can occur. In this case, both the results output by the BEP solver and the WSP solver diverged from the results of the linear solver (in particular at steeper/higher-frequency waves, with a discrepancy of up to 34%) since buoy motion induced nonlinearities (e.g. those arising from surface piercing phenomenon) became dominant in the system hydrodynamics. The BEP solver and the WSP solver output similar results, with a difference of up to 13%. In general, the WSP solver results were slightly lower than the CFD results, with a discrepancy of up to 8%. The small discrepancy can be attributed to the weak-scatterer hypothesis that disabled the WSP solver from modelling wave breaking. In conclusion, the linear solver showed poor accuracy in modelling reactive control of fully submerged point absorber in high steepness waves, whilst both the BEP solver and the WSP solvers demonstrated acceptable consistency against the CFD solver. More fundamental results (e.g. wave field data and meshing analysis) and new findings are to be shared at the IWWF workshop.

## REFERENCES

- Cummins, W.E., 1962. The impulse response function and ship motions. *Schiffstechnik*, 9, 101-109.
- Ding, B. et al., 2018, Enhancing the relative capture width of submerged point absorbing wave energy converters, in Proc. of the 4<sup>th</sup> Asian Wave and Tidal Energy Conference, 9-13 September, Taipei, Taiwan.
- Falnes, J., 2007. A review of wave-energy extraction. *Marine Structure* 20, 185-201.
- Meng, F. et al., 2017, Numerical simulation of a submerged spherical point absorber with asymmetric mass distribution, in Proc. of the 2th European Wave and Tidal Energy Conference.
- Ringwood, J.V. et al., 2014, Energy-maximizing control of wave-energy converters, *IEEE Control System Magazine* 34(5), pp. 30-55.
- Penalba, M. and Ringwood, J.V., 2016, A review of wave-to-wire models for wave energy converters, *Energies* 9, 506.
- Wuillaume, P.Y., 2019, Numerical simulation of installation operations for offshore wind farms, Doctoral thesis, Ecole Centrale de Nantes.
- Pawlowski, J.S. and Bass, D.W., 1991, A theoretical and numerical model of ship motions in heavy seas, *SNAME Transactions* 99, pp. 319-350.
- Sergiienko, N.Y., 2018, Three-tether wave energy converter: hydrodynamic modelling, performance assessment and control, Doctoral thesis, the University of Adelaide.